Journal of Energy Chemistry 57 (2021) 92–98

Contents lists available at ScienceDirect

Journal of Energy Chemistry

journal homepage: www.elsevier.com/locate/jechem

http://www.journals.elsevier.com/journal-of-energy-chemistry/

Optimizing zeolite stabilized Pt-Zn catalysts for propane dehydrogenation

Linjun Xie [a], Yuchao Chai [a], Lanlan Sun [a], Weili Dai [a], Guangjun Wu [a], Naijia Guan [a,b], Landong Li [a,b,*]

[a] School of Materials Science and Engineering & National Institute for Advanced Materials, Nankai University, Tianjin 300350, China
[b] Key Laboratory of Advanced Energy Materials Chemistry of Ministry of Education, Nankai University, Tianjin 300071, China

ARTICLE INFO

Article history:
Received 22 July 2020
Revised 25 August 2020
Accepted 30 August 2020
Available online 8 September 2020

Keywords:
Propane dehydrogenation
Zeolite
Pt-Zn/Si-Beta
Deactivation

ABSTRACT

Propane dehydrogenation (PDH) provides an alternative route to non-petroleum based propylene and eligible catalysts with good overall performance are still being explored. Herein, we report the construction of zeolite stabilized Pt-Zn catalysts Pt-Zn/Si-Beta for PDH. Characterization results from transmission electron microscopy (TEM), ultraviolet–visible (UV–vis) and Fourier transform infrared (FTIR) spectroscopy reveal that highly-dispersed Zn species are stabilized by the silanols from zeolite framework dealumination, which then act as the anchoring sites for Pt species. The close contact between Pt-Zn species and the electronic interaction thereof make Pt-Zn/Si-Beta robust PDH catalysts. Under optimized conditions, a high propylene production rate of 4.11 $molmol_{Pt}^{-1}s^{-1}$, high propylene selectivity of 98% and a sustainable deactivation rate of ~ 0.02 h^{-1} can be simultaneously achieved at 823 K. Coke deposition is not the key reason for the catalytic deactivation, while the loss of Zn species and the resulting aggregation of Pt species under high temperatures are responsible for the irreversible deactivation of Pt-Zn/Si-Beta catalyst in PDH reaction.

1. Introduction

Propylene, as an important organic intermediates of a large number of chemicals such as polymers and oxygenates [1], is mainly produced via the steam cracking of naphtha or the fluid catalytic cracking of heavy oil. However, such routes suffer from high energy consumption and produces heavy wastes [2–4]. Propane dehydrogenation (PDH) provides an alternative route to petroleum-based propylene with significant industrial relevance [4–6]. More importantly, the availability of abundant shale gas containing light alkanes makes PDH more attracting in terms of the economy and environment. Pt-based catalyst has been developed as a well-known type of catalysts that shows considerable activity for PDH reaction. It is highly desired to improve the activity of Pt-based catalysts so as to make better use of precious metal platinum and reduce the catalyst cost. On the other hand, the agglomeration of metal species during reaction or the regeneration process and the catalytic deactivation thereof should be well addressed considering potential industrial applications [7,8].

In this context, Pt-based bimetallic catalysts such as Pt-Ti [9], Pt-Ga [6,10], Pt-Cu [1], Pt-Sn [11–13], and Pt-Zn [14] have been intensively investigated in the past decades, and the Oleflex PDH process with Pt-Sn/γ-Al_2O_3 catalyst has been successfully commercialized by UOP [6]. For all cases, the introduction of the second metal species with strong interaction could significantly promote the activity and the stability of Pt species in PDH reaction [9]. Zn, a highly abundant and non-toxic metal, has been explored as a promising modifier of Pt for PDH, but receives much less attention than the post-transition-metals Ga [6,10] and Sn [11,12]. Although the introduction of a second component exhibits great potential to improve the catalytic performance and also suppress the undesired coke formation during PDH [15,16], it is still important and challenging to stabilize Pt species on the supports under the reaction conditions of high temperatures (723–923 K, to reach reasonable propane conversion levels). Notably, Weckhuysen and coworkers reported that the migration of subnanometric Pt species during PDH reaction was relevant to the deactivation of Pt-Sn catalyst than the formation of coke deposits [17]. To disperse and stabilize Pt-based bicomponent species for PDH, high-surface-area supports with abundant surface hydroxyls such as Al_2O_3 [9–11,18] or SiO_2 [19–21] are most widely used. In our previous work, bicomponent Pt-Sn species stabilized by Si-Beta zeolite has been established as a good catalyst for the oxidative dehydrogenation of propane

* Corresponding author at: School of Materials Science and Engineering & National Institute for Advanced Materials, Nankai University, Tianjin 300350, China.
E-mail address: lild@nankai.edu.cn (L. Li).

https://doi.org/10.1016/j.jechem.2020.08.058

(ODHP) [22], which exhibited high propylene productivity and good stability due to the confinement effects of Si-Beta [23–25].

In view of the known activity of Pt and Pt-Zn in PDH and the contribution of Si-Beta support from the so-called confinement effect, we herein report the design and construction of Pt-Zn/Si-Beta catalysts for PDH. High propane conversion and good stability could be simultaneously obtained at reasonable reaction temperatures, making Pt-Zn/Si-Beta zeolite a robust low-cost catalyst for industrial PDH process. We subsequently present detailed analyses on the roles of Si-Beta support, active Pt species and Zn modifier in PDH reaction. The good catalytic performance of Pt-Zn/Si-Beta in the reaction is well explained [26], and the deactivation mechanism is finally discussed.

2. Experimental

2.1. Catalyst preparation

Zn-containing zeolite Beta, i.e. Zn/Si-Beta, was prepared via a two-step post-synthesis procedure consisting of the dealumination of the H-Beta to obtain the Si-Beta material and the subsequent stabilization of Zn by the silanol defects. In a typical synthesis, commercial H-Beta zeolite (n_{Si}/n_{Al} = 13.5) was stirred in the 13 mol/L HNO_3 solution (20 mL/g zeolite) at 373 K for 20 h and then washed with deionized water until the pH value of the filtrate was neutral, producing siliceous Si-Beta material (nSi/nAl > 1800). After drying at 353 K overnight, 1.0 g Si-Beta powder was impregnated with an appropriate amount of $Zn(NO_3)_2$ in 40 mL H_2O and dried at 353 K to achieve an intimate mixture powder. The solid mixture was put into a tubular reactor and calcined at 823 K for 12 h at a heating rate of 5 K/min to derive Zn/Si-Beta zeolite. Supported Pt catalysts were prepared by the incipient wetness impregnation method. The Si-Beta or the as-synthesized Zn/Si-Beta were impregnated in the $[Pt(NH_3)_4](NO_3)_2$ solution at room temperature for 4 h. Then, the impregnated solids were dried at 353 K overnight, and calcined at 823 K for 1 h with 2 K/min heating rate to derive Pt/Si-Beta or Pt-Zn/Si-Beta zeolite, respectively. The final products were denoted as xPt-yZn/Si-Beta, where $\times$ and y represent the weight percentage (wt%) of Zn and Pt, respectively.

2.2. Catalyst characterization

The powder X-ray diffraction (XRD) measurements were performed with 2θ values between 5° and 50° at a scanning rate of 6°/min to determine the purity and the crystallinity of the catalysts, by using a Rigaku Mini Flex II diffractometer employing the graphite filtered Cu K_α radiation (λ = 1.5406 Å).

The surface areas of zeolite samples were determined by argon adsorption/desorption isotherms at 87 K collected on a Quantachrome iQ-MP gas adsorption analyzer. The Brunauer Emmett Teller (BET) method was used to calculate the total surface area and the t-plot method was employed to calculate the micropore properties.

The diffuse reflectance ultraviolet–visible (UV–vis) spectra of the dehydrated samples against $BaSO_4$ were recorded on a PerkinElmer Lambda 750 UV–Vis-NIR spectrophotometer in the range of 200–800 nm.

The Fourier transform infrared (FTIR) spectrum of zeolite samples were performed on a Bruker Tensor 27 spectrometer with 256 scans at a resolution of 2 cm^{-1}, and the spectra were recorded in the transmission-mode against KBr as the background. FTIR spectra of CO adsorption on samples were obtained with 512 scans at a resolution of 4 cm^{-1}. The samples were pretreated in He at 623 K for 1 h. After cooling to 298 K, 1 vol% CO/He gas was introduced into the system for 30 min. Then the system was purged with He and FTIR spectra of CO adsorption were sequentially recorded.

The temperature-programmed desorption was also performed on the Quantachrome ChemBET 3000 chemisorption analyzer with a mass spectrometry detector. Briefly, the sample was treated at 623 K in He for 1 h and with the reaction temperature cooled to 333 K, saturated with 5 vol% NH_3/Ar or 5 vol% C_3H_6/He). Then, the samples were purged by He flow at 333 K to eliminate the physically absorbed species and subsequently heated to target temperature with the heating rate of 10 K/min.

Transmission electron microscopy (TEM) images were obtained by a JEOL JEM-2800 transmission electron microscope at 200 KV. Mapping the elemental distribution of the samples was conducted under STEM mode using a JEOL built-in energy dispersive spectrum (EDS) software.

X-ray photoelectron spectroscopy (XPS) analyses of the samples were carried out on a Thermo Scientific ESCALAB 250Xi spectrometer with monochromatic Al-K_α X-rays as the excitation source. Accurate binding energies were determined with respect to the position of the adventitious C 1 s peak at 284.8 eV.

2.3. Catalytic evaluation

Propane dehydrogenation reaction was carried out in a quartz fixed-bed reactor with an inner diameter of 6 mm at atmospheric pressure. First, the catalyst sample (typically 0.1 g, sieve fraction of 0.25–0.5 mm) was placed in a quartz reactor, and treated in 10 vol % H_2 at 473 K for 1 h. The reactant gas mixture contained 10 vol% propane with the balance He was fed to the reactor. The weight hourly space velocity (WHSV) of propane was controlled to 2.4–6.0 h^{-1}. The reaction was conducted isothermally and the gas products were analyzed by using an on-line gas chromatograph (Agilent 7890). The conversion of propane and the selectivity toward propylene were defined as follows:

$$C_3H_8\ \text{conversion}(\%) = \frac{[C_3H_8]_{inlet} - [C_3H_8]_{outlet}}{[C_3H_8]_{inlet}} \times 100$$

$$C_3H_8\ \text{selectivity}(\%) = \frac{[C_3H_6]_{outlet}}{[C_3H_8]_{inlet} - [C_3H_8]_{outlet}} \times 100$$

3. Results and discussion

3.1. Catalyst preparation and characterization

The XRD patterns of the parent H-Beta, Si-Beta, Zn/Si-Beta, and Pt-Zn/Si-Beta are shown in Fig. 1(a). Typical diffraction lines characteristic for the BEA topology are observed for all samples, while a noticeable decline in the intensity could be observed after the introduction of Zn species. For 0.1Pt-2Zn/Si-Beta, no diffraction lines corresponding to metal oxides or alloys could be detected due to the low loadings and high dispersion of species on the support [27]. The well-preserved microporous BEA topology structure of Beta are confirmed by the argon adsorption–desorption measurement. As shown in Fig. 1(b), all samples under study showed similar type I isotherms, revealing the typical microporous structure. The detailed textural properties of Si-Beta, and M/Si-Beta samples are summarized in Table S1. All samples exhibit similar high surface areas of 553 ~ 616 $m^2\ g^{-1}$ and large micropore volumes of 0.351–0.413 $cm^3\ g^{-1}$, indicating the well preserved microporous structure of Beta zeolite after dealumination and metal incorporation. Moreover, an increase in argon absorption is observed at high relative pressure p/p_0 > 0.9, which should be attributed to the contribution of intergranular spaces caused by

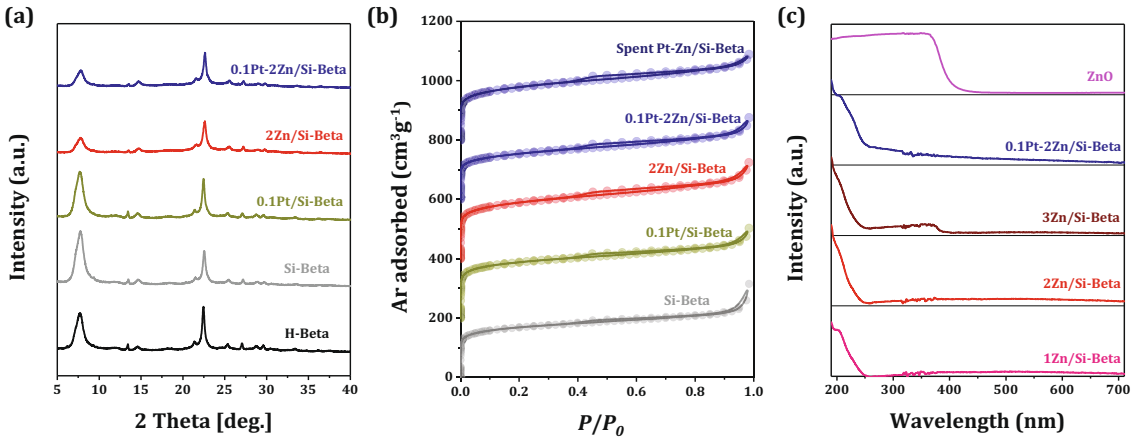

Fig. 1. Physical-chemical properties of zeolite catalysts. (a) XRD patterns of selected samples; (b) argon adsorption/desorption isotherms of selected samples; (c) UV–vis spectra of Zn-containing samples.

the disordered agglomeration of small crystallites of the Beta zeolite, as confirmed by the SEM image in Fig. S1.

In order to evaluate the chemical environment of Zn species on Si-Beta zeolite, UV–vis analysis was performed with selected samples and the corresponding spectra are shown in Fig. 1(c). In the case of ZnO, a very broad band centered at ~ 370 nm due to the ligand-to-metal charge transfer from O^{2-} to Zn^{2+} in macrocrystalline ZnO is observed [14,28,29]. For 1Zn/Si-Beta and 2Zn/Si-Beta, only the ligand-to-metal charge transfer from O^{2-} to Zn^{2+} in Si-O-Zn structure (sharp band at ~ 205 nm) could be observed, and the broad band at ~ 370 nm appears with Zn loading increase to 3%, i.e. 3Zn/Si-Beta. That is, Zn species could disperse well on Si-Beta zeolite support and the aggregation of Zn species to bulky ZnO particles could be significantly suppressed [14]. The introduction of Pt species via impregnation does not change the dispersion of Zn species on Si-Beta support.

The morphology of the zeolite support and the dispersion of Pt and Zn species on Si-Beta support were directly investigated by electron microscopy and the representative results are shown in Fig. 2. Generally, 0.1Pt-2Zn/Si-Beta appears as small aggregates of below 100 nm. In the HR-TEM image, homogeneously dispersed dark dots of 1 ~ 2.5 nm could be observed. STEM mapping analyses reveal the presence of both highly-dispersed Zn species (<1 nm) and small aggregates (1 ~ 2.5 nm). Meanwhile, no aggregation of Pt species could be observed due to its high dispersion and low loading. Obviously, Pt and Zn species appear in the overlapped locations, hinting to the close contact between Pt and Zn species on Si-Beta zeolite support.

The evolution the silanol groups after dealumination and metal incorporation procedures was monitored by infrared spectroscopy to disclosed the formation of Pt-Zn species on Si-Beta zeolite. Fig. 3 (a) shows the FTIR transmittance spectra in the framework vibration region (800 ~ 1400 cm^{-1}) of selected zeolite samples. No obvious band in the range of 900 ~ 1000 cm^{-1} occurs on H-Beta sample, while a new FTIR band center at ~ 960 cm^{-1} appear for the Si-Beta sample due to the formation of abundant silanol defects from framework dealumination [23,30,31]. Subsequently, the IR band at ~ 960 cm^{-1} disappears on 2Zn/Si-Beta with the introduction of Zn species, indicating the strong interaction between Zn species and the silanols [32]. That is, the Zn species are stabilized by interaction with silanols with the formation of Si-O-Zn linkages, as revealed by UV–vis spectra.

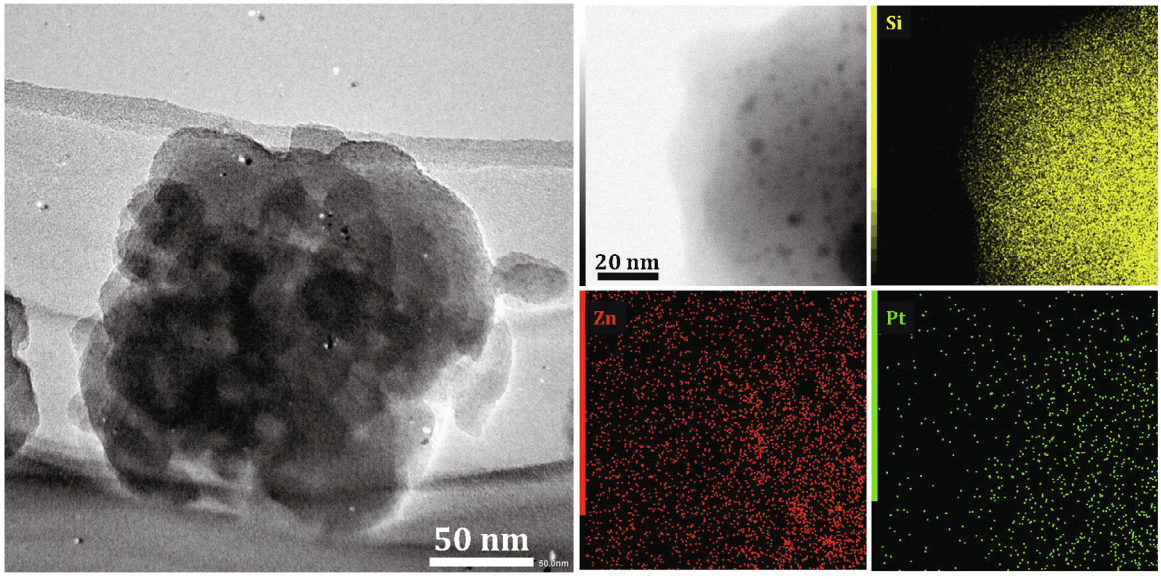

Fig. 2. TEM and STEM elemental mapping images of 0.1Pt-2Zn/Si-Beta sample.

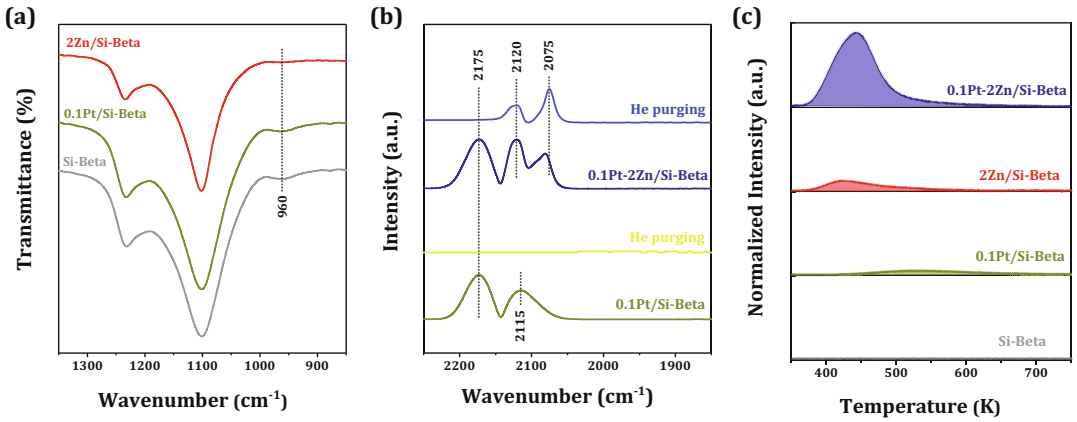

Fig. 3. Existing states of Pt and Zn in zeolites. (a) FTIR transmittance spectra of Si-Beta, Pt/Si-Beta and Zn/Si-Beta; (b) FTIR spectra of CO adsorption on Pt/Si-Beta and Pt-Zn/Si-Beta; (c) NH_3-TPD profiles of selected zeolite samples.

The local electronic environment of Pt is of great significance for PDH process. In this study, the local electronic environment of Pt was investigated by FTIR spectra of CO adsorption, which is reliable for the discrimination of highly dispersed Pt centers and large metal bulks even at very low Pt loading. As shown in Fig. 3(b), two obvious CO adsorption bands at 2115 cm^{-1} and 2175 cm^{-1} due to weakly adsorbed CO species could be observed on Pt/Si-Beta, which disappear after He purging at room temperature. In contrast, a series of IR bands are observed on 0.1Pt-2Zn/Si-Beta and two stable bands at 2120 cm^{-1} and 2075 cm^{-1} are preserved after He purging. According to literature reports [33–35], the band of 2075 cm^{-1} can be assigned to the CO molecules linearly adsorbed in an on-top geometry on Pt atoms on single-crystal or nanoparticle surfaces and the band of 2120 cm^{-1} belongs to the CO molecules linearly adsorbed on Pt single atoms. The formation of solely linearly-adsorbed CO hints to the existence of highly dispersed Pt species of 0.1Pt-2Zn/Si-Beta zeolite, in good agreement with TEM observations. Obviously, the presence of Zn is helpful for the dispersion of Pt species [36].

The acidity of Si-Beta, 0.1Pt/Si-Beta, 2Zn/Si-Beta and 0.1Pt-2Zn/Si-Beta samples were evaluated by means of NH_3-TPD and the results are shown in Fig. 3(c). Parent H-Beta demonstrates two NH_3 desorption peaks, revealing the presence of both weak and strong acid sites, respectively (not shown here) [37–41]. After the complete dealumination of H-Beta, no desorption peaks could be observed for the resulting Si-Beta sample due to the absence of acid sites [42]. Subsequently, the introduction of a small amount of Pt species to the Si-Beta support results in the appearance of trace medium acid sites (NH_3 desorption peak centered at 523 K) and the introduction of Zn results in the appearance of higher amount of Lewis acid sites (NH_3 desorption peak centered at 423 K). With the introduction of Pt into 2Zn/Si-Beta, an ammonia desorption peak centered at 443 K with much higher intensity could be observed on 0.1Pt-2Zn/Si-Beta. With electrons transfer from Zn species to Pt species, the Zn species become electron-deficient and Lewis acidic thereof. In other word, the observed Lewis acidity in 0.1Pt-2Zn/Si-Beta as compared to 2Zn/Si-Beta should indicate the strong interaction between Pt and Zn species on the Si-Beta support.

3.2. Catalytic performance in PDH

The catalytic performance of as-obtained 0.1Pt-2Zn/Si-Beta in PDH reaction, together with some other zeolite samples for reference, was thoroughly investigated. As shown in Fig. 4(a), both Si-Beta and Pt/Si-Beta exhibit very low activity in PDH reaction. That is, monometallic Pt supported on Si-Beta zeolite cannot catalyze the PDH well. 2Zn/Si-Beta appears to be active in PDH and the propane conversion of ~ 15% with ~ 90% selectivity toward propylene can be at high temperatures of > 823 K. Interestingly, upon the addition of trace Pt into 2Zn/Si-Beta zeolite, significant improvement in propane conversion and propylene selectivity can be simultaneously obtained. Typically, stable propylene selectivity of 98% and high propylene yield of 63% are achieved on 0.1Pt-2Zn/Si-Beta catalyst at 823 K.

In order to investigate the role of Zn on Pt in the bicomponent catalyst, the effects of Pt-Zn loading order on the PDH performance were further investigated. As shown in Fig. S2, 0.1Pt-2Zn/Si-Beta catalyst, with Zn loading first and Pt loading later, exhibits much better catalytic performance than the control sample 2Zn-0.1Pt/Si-Beta (Pt loading first and Zn loading later). This should be explained from the functions of pre-loaded Zn species in suppressing Pt agglomeration and Pt-Zn interaction, which are well supported by TEM observations in Figs. 2, S3 and S4 [43].

In order to obtain an optimal PDH catalyst, the effects of Pt and Zn loadings in Pt-Zn/Si-Beta catalysts on PDH performance were further investigated. As shown in Fig. 4(b), with the fixed Pt loading of 0.1%, the propane conversion on 0.1Pt-Zn/Si-Beta gradually increases with increasing Zn loading from 0.5% to 2%. Further increasing Zn loading to 3% does not bring about increasing propane conversion but results in a slight decrease instead. With fixed Zn loading of 2%, the propane conversion first dramatically increases with Pt loading increasing from 0.05% to 0.1% and then decreases distinctly with further increasing Pt loading to 0.5% (Fig. 4c). According to these observations, it is rational to propose Pt species in Pt-Zn/Si-Beta as the dominant active sites for PDH reaction although Zn species are indeed active for the reaction. An optimized Pt/Zn ratio with the close contact and electronic interaction between Pt and Zn species is essential for the success of 0.1Pt-2Zn/Si-Beta catalyst. Framework vacant sites created from dealumination, i.e. the silanol groups, can act as the anchoring sites for Zn and Pt-Zn species and therefore ensure the homogeneous dispersion of Pt-Zn species. 0.1Pt-2Zn/Si-Beta seems to be a promising low-cost PDH catalyst with very low Pt loading.

In fact, 0.1Pt-2Zn/Si-Beta is very active in PDH reaction and the propane-to-propylene conversion is very close to the equilibrium conversion at the propane partial pressure of 0.1 bar (Fig. 5a). We then investigate the deactivation behavior of 0.1Pt-2Zn/Si-Beta in PDH reaction. As shown in Fig. 5(b), a very high initial propylene production rate of 1.89 $molmol_{Pt}^{-1}s^{-1}$ with propylene selectivity of 98% is achieved for 0.1Pt-2Zn/Si-Beta at 823 K. The

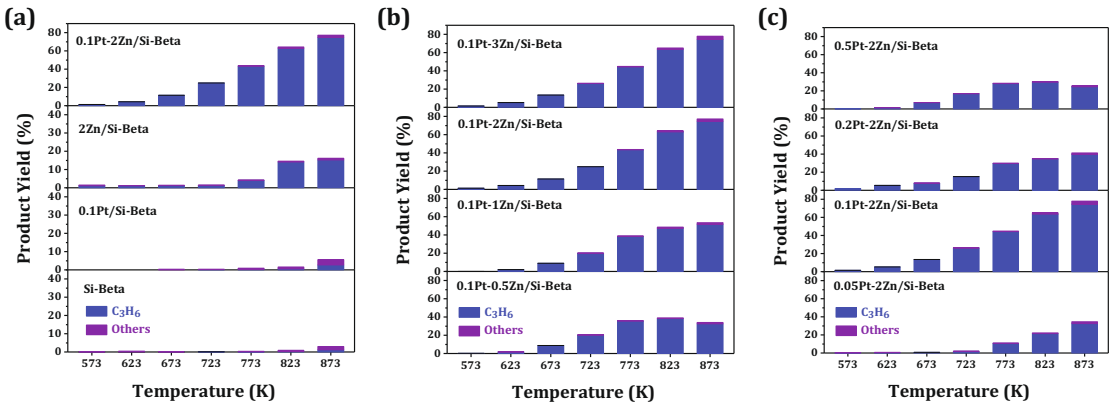

Fig. 4. Catalytic performance of selected zeolite samples in propane dehydrogenation. (a) Comparison of Si-Beta, Pt/Si-Beta, Zn/Si-Beta and Pt-Zn/Si-Beta; (b) effects of Zn loadings on the performance of Pt-Zn/Si-Beta catalysts; (c) effects of Pt loadings on the performance of Pt-Zn/Si-Beta catalysts. Reaction conditions: P = 1 bar, WHSV = 2.4 h^{-1}, C_3H_8/He = 1:9.

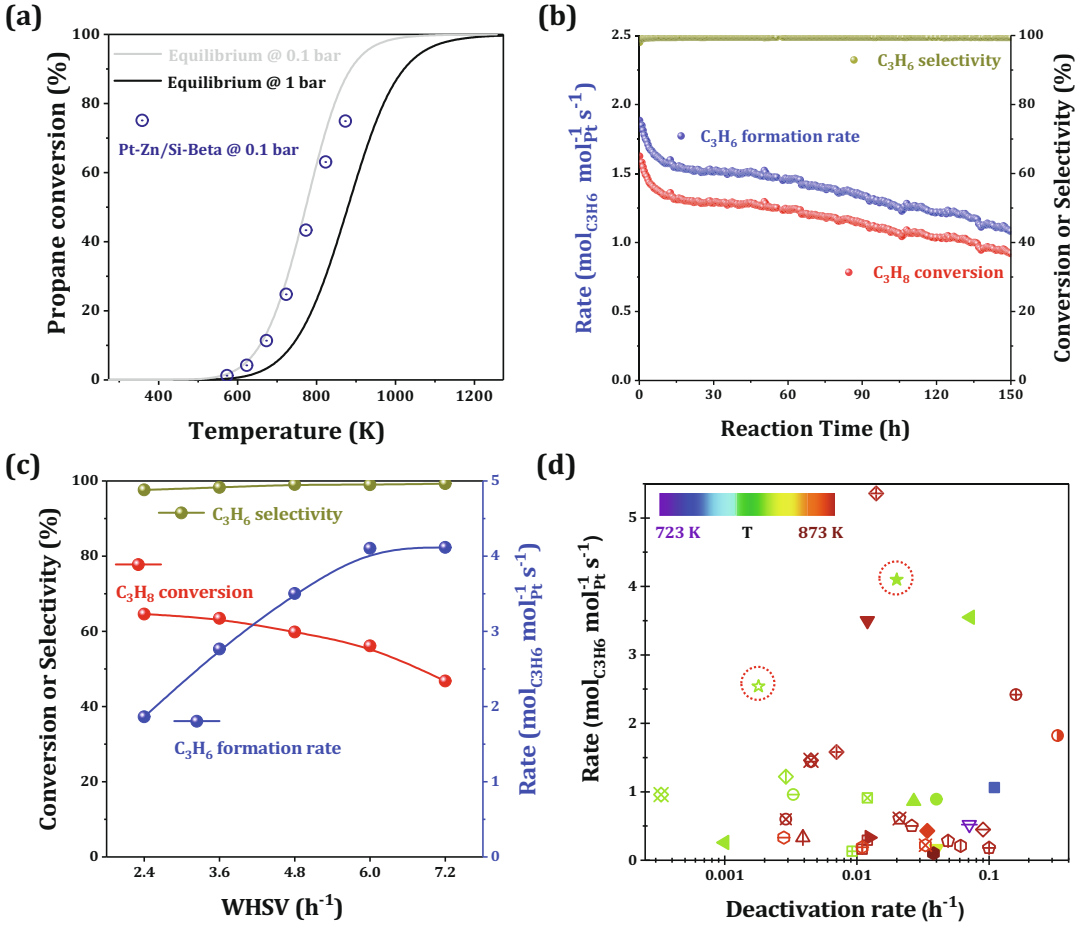

Fig. 5. Performance of optimized Pt-Zn/Si-Beta catalyst in propane dehydrogenation. (a) Temperature-dependent propane conversion over 0.1Pt-2Zn/Si-Beta catalyst, WHSV = 2.4 h^{-1}; (b) long-term stability test of 0.1Pt-2Zn/Si-Beta in propane dehydrogenation at 823 K, WHSV = 2.4 h^{-1}; (c) effects of WHSV on propane conversion, propylene selectivity and the specific activity (defined as mole of propylene formed per mole of Pt per second) over 0.1Pt-2Zn/Si-Beta; (d) comparison of the specific activity and deactivation rate in recent literature (S1 ~ 30, see Table S2 for details). Open symbols: in the presence of hydrogen; Closed symbols: in the absence of hydrogen; 0.1Pt-2Zn/Si-Beta marked by red cycles.

high propylene selectivity could be well preserved in long-term operation while propylene production rate gradually drops to 1.10 $molmol_{Pt}^{-1}s^{-1}$ within 150 h. Typically, the propylene production rate drops to 1.53 $molmol_{Pt}^{-1}s^{-1}$ (by ~ 20 %) in the first 10 h of operation and it further drops to 1.10 in the next 140 h (by ~ 22 %).

The reaction parameters in PDH catalyzed by 0.1Pt-2Zn/Si-Beta were further optimized. With increasing WHSV value from 2.4 to 7.2 h^{-1}, the propane conversion gradually decreases from 65% to 46%, while the propylene selectivity remains around 98% (Fig. 5c). On the other hand, the propylene production rate first increases with WHSV, reaches a maximum at WHSV of 6.0 h^{-1} (4.11 $molmol_{Pt}^{-1}s^{-1}$) and remains almost unchanged with the further increasing WHSV to 7.2 h^{-1}. Considering both propane conversion and propylene production rate, the WHSV value of 6.0 h^{-1} might be optimized, which is also close to the WHSV employed in Oleflex process [6]. H_2O, CO_2 and H_2 were fed to the reaction system aiming to suppress the coke formation and to prolong the catalyst lifetime in PDH. As shown in Fig. S5, H2O (5%) and CO_2 (10%) cannot prolong the catalyst lifetime while they even show great inhibition effect on PDH reaction. In contrast, although H_2 shows some negative impact on PDH reaction from the view of reaction equilibrium, it really promotes the catalyst stability to some extent probably by suppressing the deep dehydrogenation and the coke formation thereof [14,44–48].

To our knowledge, the catalytic performance 0.1Pt-2Zn/Si-Beta in PDH, in terms of activity and stability, are very attractive and a direct comparison with representative catalysts from literature is summarized in Fig. 5(d). Typically, a specific activity value, i.e. propylene production rate, of 4.11 $molmol_{Pt}^{-1}s^{-1}$ with an acceptable deactivation rate of ~ 0.02 h^{-1} is achieved with our 0.1Pt-2Zn/Si-Beta catalyst in the absence of hydrogen, while a specific activity value of 2.54 $molmol_{Pt}^{-1}s^{-1}$ with a very low deactivation rate of < 0.002 h^{-1} is achieved in the presence of H_2. These results are comparable with the best results reported for Pt-based catalysts in PDH (Fig. 5d & Table S2). The simple preparation route and the low-cost feature will further contribute to the advantages to 0.1Pt-2Zn/Si-Beta catalyst for future application.

Temperature-programmed desorption studies were performed to get some insight into intrinsic features of 0.1Pt-2Zn/Si-Beta in PDH reaction. The reactant propane appears to be weakly adsorbed on all samples, as indicated by the desorption peaks at below 523 K in Fig. 6(a). That is, the gas-phase propane directly participates in PDH reaction. On the other hand, the product propylene strongly adsorbs on 0.1Pt/Si-Beta (desorption peaks up to 723 K) and 2Zn/Si-Beta (desorption peaks up to 823 K), but weakly adsorbs on 0.1Pt-2Zn/Si-Beta (desorption peaks up to 623 K) (Fig. 6b). These results show that the modulation of Pt by Zn species, i.e. the electron transfer from Zn to Pt species, can enrich the electron density of Pt and thus weaken the electron-rich propylene adsorption [1,4]. Accordingly, the deep dehydrogenation and the formation of coke deposits can be greatly suppressed, as confirmed by the result from TG-DSC analysis in Fig. S6.

Due to the low coke content in the spent catalyst (1.61%), a simple coke-burning calcination step cannot fully regenerate 0.1Pt-2Zn/Si-Beta. Meanwhile, the BEA topology of catalyst is well preserved after PDH reaction (Fig. 1b), ruling out the catalytic deactivation due to zeolite structure destruction. The distribution of Pt and Zn species on the spent and regenerated 0.1Pt-2Zn/Si-Beta samples was then examined by electron microscopy and the representative images are shown in Fig. 7(a and b), respectively. In contrast to the fresh sample (Fig. 2), the aggregation of Pt species in spent 0.1Pt-2Zn/Si-Beta (after PDH reaction for 150 h) is confirmed by element mapping analysis. Calcination in air results in the re-dispersion of Pt species to some extent but not fully re-dispersion. The aggregation of Pt species indicates the spatial separation of Pt and Zn species and the weakening of Pt-Zn interaction [49–51], which is not good for PDH reaction. XPS analyses (Fig. 7c) indicate that Zn species in the form of Zn(II) in spent 0.1Pt-2Zn/Si-Beta catalyst, similar to the fresh sample but the Zn 2p signal is distinctly lower. Meanwhile, ICP analysis gives a Zn loading of 1.13 wt % in the spent 0.1Pt-2Zn/Si-Beta, in contrast to the value of 1.91 wt % in the fresh sample (Table S1). It is therefore proposed the loss of Zn species during the high-temperature PDH reaction, which leads

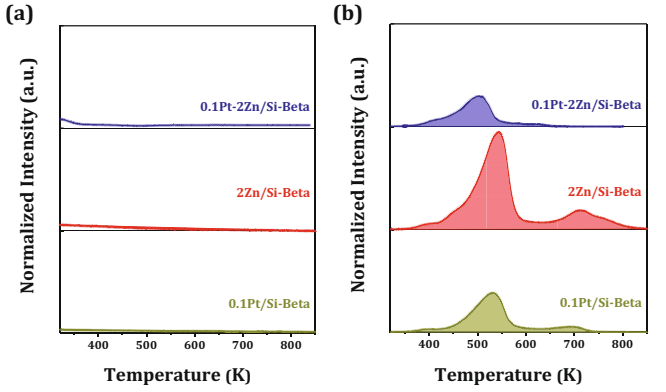

Fig. 6. Temperature-programmed desorption studies on 0.1Pt/Si-Beta 2Zn/Si-Beta, and 0.1Pt-2Zn/Si-Beta. (a) Propane desorption profiles on samples; (b) propylene desorption profiles on samples.

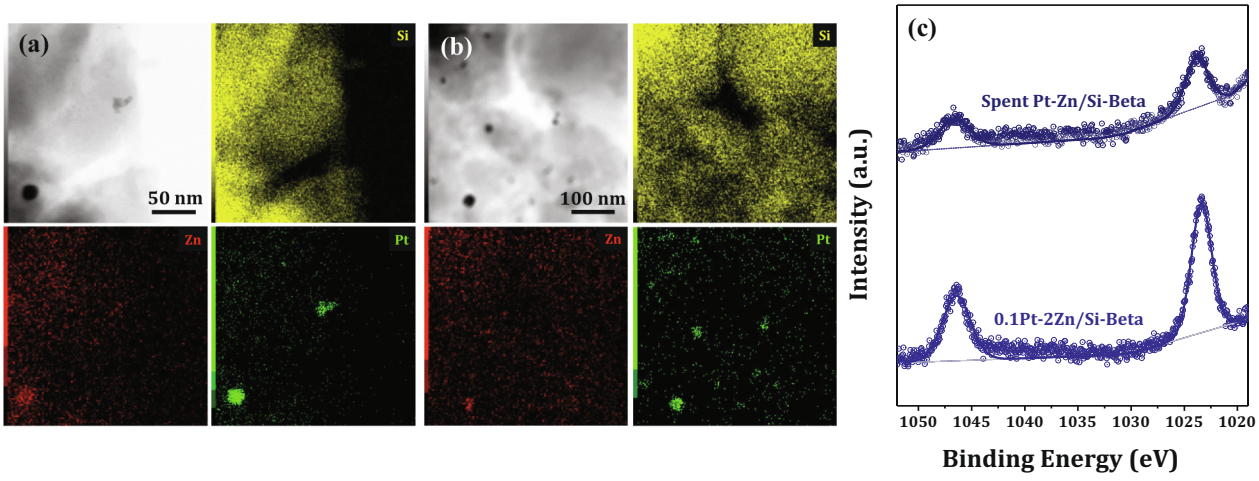

Fig. 7. Characterization of spent 0.1Pt-2Zn/Si-Beta catalyst. (a) STEM and elemental mapping of spent 0.1Pt-2Zn/Si-Beta; (b) STEM and elemental mapping of regenerated 0.1Pt-2Zn/Si-Beta; (c) Zn 2p XPS of fresh and spent 0.1Pt-2Zn/Si-Beta.

to the weakening of Pt-Zn interaction and the aggregation of Pt species in 0.1Pt-2Zn/Si-Beta.

4. Conclusions

Zeolite stabilized Pt-Zn catalysts have been prepared via a two-step post-synthesis procedure and investigated for the direct dehydrogenation of propane to propylene. Briefly, Zn species are stabilized by the silanols from zeolite framework dealumination and then act as the anchoring sites for Pt species. In such way, Pt-Zn species are highly dispersed on zeolite support with close contact and their electronic interactions are guaranteed.

The catalyst compositions and reaction parameters have been fully optimized. Very high propylene production rate of 4.11 $molmol_{Pt}^{-1}s^{-1}$, with high propylene selectivity of 98% and a sustainable deactivation rate of ~ 0.02 h^{-1}, can be achieved with 0.1Pt-2Zn/Si-Beta at 823 K. In the presence of H_2, a very low deactivation rate of < 0.002 h^{-1} with high propylene selectivity of 98 % and propylene production rate of 2.54 $molmol_{Pt}^{-1}s^{-1}$can be achieved. The good performance as well as the low-cost and easily-scalable properties makes 0.1Pt-2Zn/Si-Beta a promising PDH catalyst for future applications.

Coke deposition on 0.1Pt-2Zn/Si-Beta is found to be very low during PDH reaction, and therefore, is not the key reason for the catalytic deactivation. On the other hand, the loss of Zn species and the resulting aggregation of Pt species are clearly observed during high-temperature PDH reaction, which are proposed to be responsible for the irreversible deactivation of Pt-Zn/Si-Beta catalyst.

Declaration of Competing Interest

The authors declare that they have no known competing financial interests or personal relationships that could have appeared to influence the work reported in this paper.

Acknowledgments

This work was supported by the Municipal Natural Science Foundation of Tianjin (18JCJQJC47400, 18JCZDJC37400), National Postdoctoral Program for Innovative Talent (BX20200171) and the Fundamental Research Funds for the Central Universities.

Appendix A. Supplementary data

Supplementary data to this article can be found online at https://doi.org/10.1016/j.jechem.2020.08.058.

References

[1] Z. Han, S. Li, F. Jiang, T. Wang, X. Ma, J. Gong, Nanoscale 6 (2014) 10000–10008.
[2] J. Baek, H.J. Yun, D. Yun, Y. Choi, J. Yi, ACS Catal. 2 (2012) 1893–1903.
[3] E. Gomez, S. Kattel, B. Yan, S. Yao, P. Liu, J.G. Chen, Nat. Commun. 9 (2018) 1398.
[4] P. Sun, G. Siddiqi, M. Chi, A.T. Bell, J. Catal. 274 (2010) 192–199.
[5] H. Jowkary, M. Farsi, M.R. Rahimpour, Int. J. Hydrogen Energy 45 (2020) 7364–7373.
[6] Y. He, Y. Song, D.A. Cullen, S. Laursen, J. Am. Chem. Soc. 140 (2018) 14010–14014.
[7] F. Huang, Y. Deng, Y. Chen, X. Cai, M. Peng, Z. Jia, J. Xie, D. Xiao, X. Wen, N. Wang, Z. Jiang, H. Liu, D. Ma, Nat. Commun. 10 (2019) 4431–4437.
[8] F. Huang, Y. Deng, Y. Chen, X. Cai, M. Peng, Z. Jia, P. Ren, D. Xiao, X. Wen, N. Wang, Z. Jiang, H. Liu, D. Ma, J. Am. Chem. Soc. 140 (2018) 13142–13146.
[9] F. Jiang, L. Zeng, S. Li, G. Liu, S. Wang, J. Gong, ACS Catal. 5 (2014) 438–447.
[10] J. Im, M. Choi, ACS Catal. 6 (2016) 2819–2826.
[11] A. Iglesias-Juez, A.M. Beale, K. Maaijen, T.C. Weng, P. Glatzel, B.M. Weckhuysen, J. Catal. 276 (2010) 268–279.
[12] L. Liu, M. Lopez-Haro, C.W. Lopes, C. Li, P. Concepcion, L. Simonelli, J.J. Calvino, A. Corma, Nat. Mater. 18 (2019) 866–873.
[13] J. Zhang, Y. Deng, X. Cai, Y. Chen, M. Peng, Z. Jia, Z. Jiang, P. Ren, S. Yao, J. Xie, D. Xiao, X. Wen, N. Wang, H. Liu, D. Ma, ACS Catal. 9 (2019) 5998–6005.
[14] G. Liu, L. Zeng, Z.-J. Zhao, H. Tian, T. Wu, J. Gong, ACS Catal. 6 (2016) 2158–2162.
[15] J.J. Sattler, J. Ruiz-Martinez, E. Santillan-Jimenez, B.M. Weckhuysen, Chem. Rev. 114 (2014) 10613–10653.
[16] H. Song, R.M. Rioux, J.D. Hoefelmeyer, R. Komor, K. Niesz, M.E. Grass, P. Yang, G.A. Somorjai, J. Am. Chem. Soc. 128 (2006) 3027–3037.
[17] H.N. Pham, J.J. Sattler, B.M. Weckhuysen, A.K. Datye, ACS Catal. 6 (2016) 2257–2264.
[18] S. Zhou, Y. Zhou, J. Shi, Y. Zhang, X. Sheng, Z. Zhang, J. Mater. Sci. 50 (2015) 3984–3993.
[19] G. Wang, H. Zhang, H. Wang, Q. Zhu, C. Li, H. Shan, J. Catal. 344 (2016) 606–608.
[20] K. Searles, K.W. Chan, J.A. Mendes Burak, D. Zemlyanov, O. Safonova, C. Coperet, J. Am. Chem. Soc. 140 (2018) 11674–11679.
[21] N.M. Schweitzer, B. Hu, U. Das, H. Kim, J. Greeley, L.A. Curtiss, P.C. Stair, J.T. Miller, A.S. Hock, ACS Catal. 4 (2014) 1091–1098.
[22] L. Sun, Y. Chai, W. Dai, G. Wu, N. Guan, L. Li, Catal, Sci. Technol. 8 (2018) 3044–3051.
[23] S. Song, G. Wu, W. Dai, N. Guan, L. Li, Catal Sci. Technol. 6 (2016) 8325–8335.
[24] Y. Chai, L. Xie, Z. Yu, W. Dai, G. Wu, N. Guan, L. Li, Micropor. Mesopor. Mater. 264 (2018) 230–239.
[25] D. Yu, W. Dai, G. Wu, N. Guan, L. Li, Chin. J. Catal. 40 (2019) 1375–1384.
[26] C. Yu, H. Xu, Q. Ge, W. Li, J. Mol. Catal. A. 266 (2007) 80–87.
[27] S. Wang, K. Gao, W. Li, J. Zhang, Appl. Catal. A. 531 (2017) 89–95.
[28] J. Chen, Z. Feng, P. Ying, C. Li, J. Phys. Chem. B. 108 (2004) 12669–12676.
[29] Y.G. Kolyagin, V.V. Ordomsky, Y.Z. Khimyak, A.I. Rebrov, F. Fajula, I.I. Ivanova, J. Catal. 238 (2006) 122–133.
[30] G.G. Juttu, R.F. Lobo, Catal. Lett. 62 (1999) 99–106.
[31] T.D. Courtney, C.-C. Chang, R.J. Gorte, R.F. Lobo, W. Fan, V. Nikolakis, Micropor. Mesopor. Mater. 210 (2015) 69–76.
[32] M.A. Camblor, A. Corma, J. Pérez-Pariente, J. Chem. Soc., Chem. Commun. (1993) 557–559.
[33] A.D. Allian, K. Takanabe, K.L. Fujdala, X. Hao, T.J. Truex, J. Cai, C. Buda, M. Neurock, E. Iglesia, J. Am. Chem. Soc. 133 (2011) 4498–4517.
[34] K. Ding, A. Gulec, A.M. Johnson, N.M. Schweitzer, G.D. Stucky, L. Marks, P.C. Stair, Science 350 (2019) 189–192.
[35] J. Fu, J. Lym, W. Zheng, K. Alexopoulos, A.V. Mironenko, N. Li, J.A. Boscoboinik, D. Su, R.T. Weber, D.G. Vlachos, Nat. Catal. 3 (2020) 446–453.
[36] Q. Sun, N. Wang, Q. Fan, L. Zeng, A. Mayoral, S. Miao, R. Yang, Z. Jiang, W. Zhou, J. Zhang, T. Zhang, J. Xu, P. Zhang, J. Cheng, D.C. Yang, R. Jia, L. Li, Q. Zhang, Y. Wang, O. Terasaki, J. Yu, Angew. Chem. Int. Ed. 59 (2020), https://doi.org/10.1002/anie.202003349.
[37] C. Freitas, N.S. Barrow, V. Zholobenko, Johnson Matthey, Technol. Rev. 6 (2018) 279–290.
[38] C.J. Baranowski, M. Roger, A.M. Bahmanpour, O. Krocher, ChemSusChem. 12 (2019) 4421–4431.
[39] H. Fujita, T. Kanougi, T. Atoguchi, Appl. Catal. A. 313 (2006) 160–166.
[40] W. Zhang, P.G. Smirniotis, M. Gangoda, R.N. Bose, J. Phys. Chem. B. 104 (2000) 4122–4129.
[41] R.B. Borade, A. Clearfield, J. Phys. Chem. 96 (1992) 6729–6737.
[42] G.H. Kuehl, H.K.C. Timken, Micropor. Mesopor. Mater. 35–36 (2000) 521–532.
[43] B.K. Vu, M.B. Song, I.Y. Ahn, Y.-W. Suh, D.J. Suh, W.-I. Kim, H.-L. Koh, Y.G. Choi, E.W. Shin, Appl. Catal. A. 400 (2011) 25–33.
[44] T. Waku, J.A. Biscardi, E. Iglesia, Chem. Commun. 14 (2003) 1764–1765.
[45] Y. Zhang, Y. Zhou, L. Huang, M. Xue, S. Zhang, Ind. Eng. Chem. Res. 50 (2011) 7896–7902.
[46] J. Salmones, J.-A. Wang, J.A. Galicia, G. Aguilar-Rios, J. Mol. Catal. A. 184 (2002) 203–213.
[47] Y. Duan, Y. Zhou, Y. Zhang, X. Sheng, M. Xue, Catal. Lett. 141 (2010) 120–127.
[48] G. Siddiqi, P. Sun, V. Galvita, A.T. Bell, J. Catal. 274 (2010) 200–206.
[49] S. Kuld, C. Conradsen, P.G. Moses, I. Chorkendorff, J. Sehested, Angew. Chem., Int. Ed. 53 (2014) 5941–5945.
[50] W. Dai, S. Zhang, Z. Yu, T. Yan, G. Wu, N. Guan, L. Li, ACS Catal. 7 (2017) 3703–3706.
[51] M. Ismail, M.K. Rahmani, S.A. Khan, J. Choi, F. Hussain, Z. Batool, A.M. Rana, J. Lee, H. Cho, S. Kim, Appl. Surf. Sci. 498 (2019) 143833–143841.